Date of publication xxxx 00, 0000, date of current version xxxx 00, 0000.

Digital Object Identifier 10.1109/ACCESS.2023.0322000

A Distributed Sensor-based Recursive Framework for DoA Estimation and Geolocation

LEI JIANG[1],(Student Member, IEEE), NOPPHON KEERATIVORANAN[1], (Member, IEEE), TAD MATSUMOTO[1,2],(Life Fellow, IEEE) and JUN-ICHI TAKADA[1], (Senior Member, IEEE)

[1]The authors are with the Department of Transdisciplinary Science and Engineering, Tokyo Institute of Technology, Tokyo 152-8552, JAPAN (e-mail: jiang.l.ad@m.titech.ac.jp; nopphon.keerativoranan@ap.ide.titech.ac.jp; matumoto@jaist.ac.jp; takada@tse.ens.titech.ac.jp).

[2]T. Matsumoto is with IMT Atlantique, CNRS UMR 6285, Lab-STICC, Brest, France, JAIST and University of Oulu (Emeritus) (e-mail: matumoto@jaist.ac.jp).

Corresponding author: Lei Jiang (e-mail: jiang.l.ad@m.titech.ac.jp).

This work was supported in part by the Hitachi,Ltd., and in part by the Hitachi Kokusai Electric Inc.

ABSTRACT This paper proposes a distributed sensor-based RECursive Subspace and Factor Graph (REC-SaFG) framework for direction-of-arrival (DoA) estimation and geolocation of a fast-moving target. The whole framework includes two recursive processes: (1) DoA estimation and tracking by 2-dimensional (2D) smoothing-based recursive subspace technique using low rank adaptive filter (LORAF); (2) Factor graph (FG)-based geolocation and tracking network utilizing an extended Kalman filter (EKF) which takes into account the target's position and velocity, and updates them as well as the acceleration information. In (1), the recursive subspace technique aims to fully utilize sample size insufficiency due to the fast-moving target and to recover the rank deficiency incurred by the coherent signal components. In (2), the estimated DoA and target velocity information obtained by (1) is considered as input to the unified FG implemented by EKF for geolocation and tracking (FG-GE-TR) of the target position. By integrating these two processes, the REC-SaFG framework promises significant improvements in the accuracy and efficiency of geolocation and tracking systems, particularly in environments characterized by a fast-moving target and the need for high-resolution tracking.

INDEX TERMS Direction-of-arrival (DoA), geolocation, tracking, extended Kalman filter (EKF), subspace, eigenvalue decomposition (EVD), factor graph (FG), distributed sensors, low-rank adaptive filter (LORAF).

I. INTRODUCTION

RECENTLY, distributed sensor-based wireless geolocation has played significant roles in fifth-generation (5G) communications and is expected to be of even greater significance in beyond 5G (B5G) communications and sensing systems [1], [2]. In a distributed sensor network, unified location and communication services encompass signal processing at the sensing level, geolocation algorithm design at the fusion level, and decision-making based on geolocation at the decision level. The incorporation of edge computing in distributed sensor networks paves the way for the progression towards increasingly sophisticated geolocation services [3]. Edge computing, which processes data near the source instead of centralized data centers, aligns with advanced wireless geolocation needs. By distributing the computational load across the network, edge computing not only reduces latency and bandwidth usage but also enhances the reliability and speed of decision-making processes [4]. Recognizing the effectiveness of the edge computing principle, the three levels are distributed yet play their roles in a unified manner in many applications, such as autonomous driving systems, modern aviation navigation and control systems, emergency services in Enhanced 911 (E911), and drones or unmanned aerial vehicles (UAVs) for smart cities [5]- [8].

The conventional technique used in geolocation systems, such as the Global Positioning System (GPS) [9], utilizes trilateration. This technique determines the position of the target by measuring the distances between the target and at least three distinct satellites. This method, typically associated with time-of-arrival (ToA) techniques, requires precise temporal synchronization between the sensor network and the target to ensure the accuracy of geolocation [10], [11]. The challenge of maintaining such perfect synchronization across various devices is a significant limitation of ToA-based systems. In contrast, some systems use time difference-of-arrival (TDoA) techniques [12], [13], which compare the arrival time of a signal in different sensors to determine the location of the target. Although TDoA-based methods alleviate some of the synchronization burdens by focusing on the difference in signal arrival time rather than their absolute time, they often

require complex calculations involving hyperbolic equations and root analysis [14], [15]. This complexity can lead to constraints in estimation performance, particularly in the environments where signal propagation may be affected by various factors, such as obstacles or atmospheric conditions.

Given the limitations of trilateration-based geolocation methodologies, triangulation techniques that utilize the direction-of-arrival (DoA) of signals present a compelling alternative. The DoA-based geolocation methodology [16], [17] determines the angle at which a sensor receives a signal, enabling the calculation of the target position relative to the known sensor coordinates. Unlike ToA-based techniques, DoA-based geolocation significantly simplifies the synchronization requirement, making it necessary only at the sensor level [18]. This advantage is of particular significance in distributed sensor networks, where managing time synchronization among a large number of sensor nodes may be impractical. Furthermore, DoA methods focus on the angle of signal arrival rather than the distance. This approach makes them inherently less susceptible to errors caused by signal delay or distortion.

Over the past few decades, traditional block-wise subspace-based methods for DoA estimation, such as MUSIC and ESPRIT [19] - [22], have relied on the assumptions of the time-domain stationarity and incoherent signals to ensure the estimation accuracy. However, these assumptions do not hold in high mobility scenarios [23], resulting in a trade-off between accuracy and measurement duration. Furthermore, the block-wise process is computationally inefficient for continuous DoA tracking due to the necessity of performing repeatedly the eigenvalue decomposition (EVD) on empirical covariance matrices [24]. Recently, it has been shown that machine learning approaches, using architectures such as ResNet and CNN [25], [26], can improve the DoA estimation accuracy and robustness but they face challenges such as high computational demands and sensitivity to training data quality.

In DoA-based geolocation systems, the mathematical framework is nonlinear, which makes the direct computation complicated. To address the nonlinear trigonometric relationship between DoA measurements and position estimates, [27] introduces a maximum likelihood (ML) method, which maximizes a likelihood function derived from DoA measurements to determine the target position. Although accurate estimation can be achieved under ideal conditions, the ML method requires significant computational effort. To reduce complexity, [28] proposes a Taylor series (TS) linearization-based method to calculate the least squares (LS) solution using an initial guess. However, this method struggles with convergence if the initial guess is far from the true value. To balance accuracy and computational burden, [29] proposes a factor graph (FG)-based probabilistic model that iteratively computes the most probable locations using message passing algorithms.

To compensate for the disadvantages commonly found in conventional DOA estimation and geolocation algorithms, this paper proposes a RECursive Subspace and Factor Graph-based (REC-SaFG) framework. The whole framework includes two steps: (1) DoA estimation and tracking using recursive two-dimensional (2D) smoothing-based subspace techniques; (2) geolocation and tracking using a unified FG integrating DoA estimates from (1). In (1), the recursive 2D smoothing method first restructures the empirical covariance matrix into a smaller rectangular form by merging samples from the spatial and temporal domains [24]. This process aims to decorrelate coherent signals by using finite snapshots in empirical nonstationarity environments. Given the large size of the 2D smoothed covariance matrix due to the merging process and the relatively small number of signal sources, the problem turns into a classic low-rank case. Therefore, we integrate a low-rank adaptive filter (LORAF) algorithm [31] for consistently tracking the subspace structure, enabling continuous DoA tracking of a high mobility target.

In the geolocation and tracking part of REC-SaFG, a unified FG implemented with an extended Kalman filter (EKF) [16], [32] is proposed for the geolocation part (FG-GE) and tracking part (FG-GE-TR). The estimated DoA and velocity information obtained by the recursive subspace technique are used as input to FG-GE. After the recursive processing in FG-GE, the output position message is utilized as the observation state to refine the prediction state obtained from the *a prior* information by EKF, as in [5], [16]. The acceleration component is integrated into FG-GE-TR, enabling it to not only predict but also dynamically update the velocity. This technique effectively mitigates the limitations associated with slow motion tracking, as highlighted in [5], [16]. To ensure system stability during the high mobility tracking phase, FG-GE-TR incorporates two types of forgetting factors. One is designed to balance the weight between changes in distance and velocity. The other aims to equilibrate the significance between the velocity as an observational state derived from the recursive subspace method and the velocity as a previous state from FG-GE-TR. The values of these forgetting factors can be flexibly adjusted to accommodate various practical scenarios. The main contribution of this paper is summarized as follows:

- A two-step recursive framework, REC-SaFG, is proposed for DoA estimation and geolocation of a fast-moving target. The first step uses a recursive subspace algorithm to estimate and track DoA at each sensor. Then the estimated DoA of each sensor is sent to the fusion center for geolocation and tracking in the second step.
- In the DoA estimation and tracking part, a recursive 2D smoothing is used to decorrelate the coherent multipath components. By combining with the LORAF algorithm, the recursive subspace technique can dynamically track the DoA and minimize the smoothing effort.
- In the geolocation and tracking part, a unified FG combined with the EKF is proposed. The accuracy is improved by taking into account the updated velocity as well as the acceleration. The stability of the FG structure

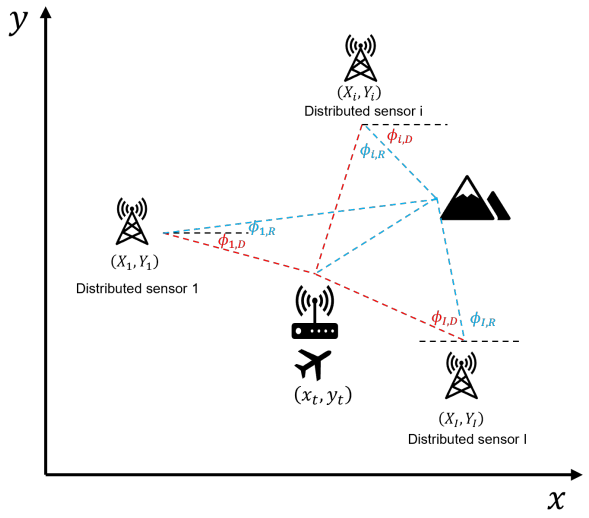

FIGURE 1. 2D geolocation of one aircraft with *I* distributed sensors

is maintained by introducing two forgetting factors to balance the output of the EKF and new observations.

The organization of this paper is as follows. The signal model for the DoA estimation and tracking model is described in Section II. In Section III, the proposed recursive DoA estimation and geolocation framework, REC-SaFG, is detailed with a recursive 2D smoothing-based subspace technique and the iteration process in FG-GE-TR. The proposed recursive framework is evaluated by a series of simulations, and the results are presented in Section IV. Finally, the conclusion of this contribution is provided in Section V.

II. SYSTEM MODEL

A geolocation and tracking system for a fast-moving aircraft located with a two-dimensional (2D) coordinate $(x_t, y_t)^T$ is considered, as shown in Fig. 1, where $[\cdot]^T$ denotes matrix transportation and t is the time index in the tracking phase. I distributed sensors, each with an M-element uniform linear array (ULA), are located at $[X_i, Y_i]^T$, where $i \in (1, \cdots, I)$ is the sensor index. Distributed sensors are managed to detect the narrowband signal with two coherent paths[1] sent from the aircraft. The estimated DoAs of two paths are denoted as $(\phi_{i,\mathrm{D}}, \phi_{i,\mathrm{R}})$, where subscripts D and R refer as direct path and reflect path.

A. SIGNAL MODEL

For the simplicity, the sensor index i is omitted unless required. At m-th element of the ULA in each sensor, the received signal is given by:

$$r_m(n_1, n\triangle T) = s_{f_{\mathrm{d_D}}}(n_1, n\triangle T)e^{-\mathrm{j}2(m-1)\pi\frac{d}{\lambda}\sin\phi_{\mathrm{D}}} + w_{\mathrm{D}}(n\triangle T) + s_{f_{\mathrm{d_R}}}(n_1, n\triangle T)e^{-\mathrm{j}2(m-1)\pi\frac{d}{\lambda}\sin\phi_{\mathrm{R}}} + w_{\mathrm{R}}(n\triangle T) \tag{1}$$

[1]To theoretically analyze the impact of the empirical nonstationarity in [23], the propagation model of the two-path, one direct, and the other coherent reflect path is used. To keep consistency of the whole framework, the same two-path model is used in this paper as well.

where $n \in \{1, \cdots, N\}$ and $\triangle T$ denote the snapshot index and the sampling interval, respectively. n_1 is the initial sampling point that is used to evaluate the impact of empirical nonstationarity in [23]. d and λ present the element spacing and the wavelength, respectively. $w_{\{\mathrm{D,R}\}}(n\Delta T)$ is the additional white Gaussian noise (AWGN). $s_{f_{\mathrm{d_D}}}(n_1, n\triangle T)$ is the wavefront corresponding to the Doppler frequency of the direct path, defined as:

$$s_{f_{\mathrm{d_D}}}(n_1, n\triangle T) = \beta_{\mathrm{D}}e^{-\mathrm{j}\Phi_{\mathrm{D}}}e^{\mathrm{j}2\pi f_{\mathrm{d_D}}(n_1+n)\triangle T} \tag{2}$$

where β_{D} is the amplitude, Φ_{D} is the phase reference, and $f_{\mathrm{d_D}}$ is the Doppler frequency. The wavefront of the reflect path can be defined in the same way. Consider all M elements and use the vector to present (1):

$$\mathbf{r}(n_1, n\triangle T, m) = \mathbf{A}(\boldsymbol{\phi})\boldsymbol{\beta}(n_1)\mathbf{A}(\mathbf{f}_{\mathrm{d}}) \tag{3}$$

where $[\cdot]^H$ denotes the Hermitian transform, $\mathbf{A}(\boldsymbol{\phi}) = [\mathbf{a}(\phi_{\mathrm{D}}), \mathbf{a}(\phi_{\mathrm{R}})]$ and $\mathbf{A}(\mathbf{f}_{\mathrm{d}}) = [\mathbf{a}(f_{\mathrm{d_D}}), \mathbf{a}(f_{\mathrm{d_R}})]^H$ are steering vectors correspond to the DoAs and the Doppler frequency, respectively, and

$$\boldsymbol{\beta}(n_1) = \begin{bmatrix} \beta_D e^{-\mathrm{j}\Phi_{\mathrm{D}}}e^{\mathrm{j}2\pi f_{\mathrm{d_D}}n_1\triangle t} & \\ & \beta_R e^{-\mathrm{j}\Phi_{\mathrm{R}}}e^{\mathrm{j}2\pi f_{\mathrm{d_R}}n_1\triangle t} \end{bmatrix} \tag{4}$$

denotes the residual part including the amplitude, the initial sampling point components. Note that the recursive subspace-based technique is provided for estimating the DoA of each path in the next section. In triangulation-based geolocation techniques, only the DoA of the direct path is useful because it provides the most accurate and unambiguous information about the target position, avoiding errors introduced by multipath signals. Therefore, an association technique used to identify the DoA of the direct path is provided in the next section as well.

B. INTEGRATING DOA TO GEOLOCATION

The trigonometric express between the estimated DoA of the direct path and the aircraft location is given by:

$$\phi_{i,D} = h_i(x_t, y_t) + u_{i,t} \tag{5}$$

with the DoA estimation error $u_{i,t} \sim \mathcal{N}(0, \sigma_\phi^2)$ and $h_i(x_t, y_t)$ the true DoA, given by:

$$h_i(x_t, y_t) = \arctan\left(\frac{Y_i - y_t}{X_i - x_t}\right) \tag{6}$$

Note that the DoA estimation error is assumed to be Gaussian distributed from the MUSIC algorithm which is used in this paper. It is difficult to provide strict proof due to the peak search process of the MUSIC algorithm. Instead, we provided the empirical results by performing a Monte Carlo simulation in Chapter IV.

For the aircraft tracking phase, a nonlinear discrete state-space model (SSM) is used in this paper. The current state of the target at time $t = \{1, \cdots, T\}$ is $\mathbf{s}_t = [x_t, y_t]^T$. Similar to [16], the dynamic SSM is given by:

$$\mathbf{s}_t = f(\mathbf{s}_{t-1}) + \mathbf{e}_t \tag{7}$$

where $f(\cdot)$ denotes the nonlinear function between two adjacent states, and $\mathbf{e}_t = [e_{x,t}, e_{y,t}]^T$ is the AWGN vector. The first-order Taylor series (TS) expansion is first of all used to approximate $f(\cdot)$ to keep the message over FG Gaussianity, given by:

$$f(\mathbf{s}_{t-1}) \approx f(\boldsymbol{\gamma}) + f^{'}(\boldsymbol{\gamma})(\mathbf{s}_{t-1} - \boldsymbol{\gamma}) \tag{8}$$

with $\boldsymbol{\gamma}$ the center point of TS expansion. $f(\boldsymbol{\gamma})$ corresponds to the previous state $\mathbf{s}_{t-1}$ and the derivative $f^{'}(\boldsymbol{\gamma})(\mathbf{s}_{t-1} - \boldsymbol{\gamma})$ is the relative distance between $\mathbf{s}_{t-1}$ and $\mathbf{s}_t$, given by:

$$f^{'}(\boldsymbol{\gamma})(\mathbf{s}_{t-1} - \boldsymbol{\gamma}) = \mathbf{v}_{t-1} \cdot \triangle t \tag{9}$$

where $\mathbf{v}_{t-1} = [v_{x,t-1}, v_{y,t-1}]^T$ is the velocity, given by:

$$\mathbf{v}_{t-1} = \mathbf{v}_{t-2} + \mathbf{a}_{t-1} \cdot \triangle t \tag{10}$$

where $\mathbf{a}_{t-1}$ denotes the acceleration components. The velocity and the acceleration are updated by the EKF. We normalize the relative time $\triangle t = 1$, then (7) can be further expressed as:

$$\mathbf{s}_t \approx \mathbf{s}_{t-1} + \mathbf{v}_{t-1} + \mathbf{e}_t \tag{11}$$

In the FG-GE-TR framework, the output of FG-GE is used as the observation to refine the prediction of FG-EKF. The observation $\mathbf{j}_t$ is then given by:

$$\mathbf{j}_t = g(\mathbf{s}_t) + \mathbf{z}_t, \tag{12}$$

where $g(\mathbf{s}_t)$ returns the output of the FG-GE and $\mathbf{z}_t \sim \mathcal{N}(0, \sigma_z^2)$ denotes the observation noise which is unknown to the system. Instead, the smallest value of σ_z^2 achieved analytically by calculating the CRLB [16] is used in the FG.

III. RECURSIVE FRAMEWORK REC-SAFG

In this paper, we propose a recursive framework that connects DoA estimation, geolocation, and tracking together, as shown in Fig. 2. The whole framework includes two parts: (1) recursive DoA estimation and tracking; (2) recursive geolocation and tracking. To capture the signals from the target aircraft, distributed sensors consisting of the ULA are utilized. The 2D smoothing technique, which performs smoothing processes in both the spatial and the time domains, is used to decorrelate the coherent signal components. A recursive subspace technique with the LORAF algorithm, LORAF-MUSIC, is used to estimate and track the DoAs. Next, to extract the DoAs of the direct path from the multipath, a distance-angle-based association method is utilized. The output of the LORAF-MUSIC algorithm is then sent to the fusion center where the FG-GE-TR is performed to update the location, velocity, and acceleration information of the target.

A. RECURSIVE 2D SMOOTHING-BASED SUBSPACE TECHNIQUE FOR DOA ESTIMATION

To realize the recursion, the total N snapshots are divided into $N^{'}$ segments. Each segment has $\frac{N}{N^{'}}$ snapshots. Next, perform smoothing processes both in the spatial and temporal domains in the $n^{'}$-th segment by setting the smoothing subrectangular size to $M_0 \times N_0$, as shown in Fig. 3. In total, there are $P \times Q$ subrectangulars, which $P = M - M_0 + 1$ is the number of subarrays and $Q = \frac{N}{N^{'}} - N_0 + 1$ is the number of subsnapshots, respectively. The received signal at the p,q-th $(p = 1, \cdots, P; q = 1, \cdots, Q)$ subrectangular is given by:

$$\mathbf{r}_{p,q}^{n^{'}}(n_1) = \mathbf{A}(\phi)\mathbf{D}^{(p-1)}\boldsymbol{\beta}(n_1)\left[\mathbf{A}(\mathbf{f}_{\mathrm{d}})\mathbf{C}^{(q-1)}\right]^H \tag{13}$$

where $\mathbf{D}^{(p)}$ and $\mathbf{C}^{(q)}$ are the p-th power of the shift matrix $\mathbf{D}$ and the q-th power of the shift matrix $\mathbf{C}$, respectively, given by:

$$\mathbf{D} = \mathrm{diag}(d_{\mathrm{D}}, d_{\mathrm{R}}), \tag{14a}$$
$$\mathbf{C} = \mathrm{diag}(c_{\mathrm{D}}, c_{\mathrm{R}}), \tag{14b}$$

where

$$d_{\mathrm{D}} = e^{-\mathrm{j}2\pi\frac{d}{\lambda}\sin\phi_{\mathrm{D}}}, \tag{15a}$$
$$c_{\mathrm{D}} = e^{-\mathrm{j}2\pi f_{d_{\mathrm{D}}}\triangle T}. \tag{15b}$$

In order to conduct smoothing in two different domains, the vectorization operation is utilized to combine the spatial steering vector $\mathbf{A}(\phi)$ and the temporal steering vector $\mathbf{A}(\mathbf{f}_{\mathrm{d}})$ together, given by:

$$\begin{aligned}\mathbf{r}_{2\mathrm{D}(p,q)}^{n^{'}}(n_1) &= \mathbf{A}(\boldsymbol{\theta})\Diamond\mathbf{A}(\mathbf{f}_{\mathrm{d}})\mathrm{diag}\left(\mathbf{D}^{(p-1)}\boldsymbol{\beta}(n_1)\mathbf{C}^{(q-1)}\right) \\ &\triangleq \mathbf{A}(\boldsymbol{\theta}, \mathbf{f}_{\mathrm{d}})\boldsymbol{\alpha}(n_1)\end{aligned} \tag{16}$$

where $\Diamond$ denotes the column-wise Kronecker product, $\mathrm{diag}(\cdot)$ is the diagonalization. The $\frac{MN}{N^{'}} \times 2$ vectorized steering vector $\mathbf{A}(\boldsymbol{\theta}, \mathbf{f}_{\mathrm{d}})$ is parameterized by the DoA and the Doppler frequency.

The covariance matrix at the p,q-th subrectangular is given by:

$$\mathbf{R}_{2\mathrm{D}(p,q)}^{n^{'}}(n_1) = \mathbf{r}_{2\mathrm{D}(p,q)}^{n^{'}}(n_1)\mathbf{r}_{2\mathrm{D}(p,q)}^{n^{'}H}(n_1). \tag{17}$$

Then take average over all subrectangulars to calculate 2D smoothed covariance in $n^{'}$-th segment, given by:

$$\begin{aligned}\overline{\mathbf{R}}_{2\mathrm{D}}^{n^{'}}(n_1) &= \frac{1}{PQ}\sum_{p=1}^{P}\sum_{q=1}^{Q}\mathbf{R}_{2D(p,q)}^{n^{'}}(n_1) \\ &= \mathbf{A}(\boldsymbol{\theta}, \mathbf{f}_{\mathrm{d}})\overline{\mathbf{S}}_{2\mathrm{D}}(n_1)\mathbf{A}^H(\boldsymbol{\phi}, \mathbf{f}_{\mathrm{d}})\end{aligned} \tag{18}$$

where

$$\overline{\mathbf{S}}_{2\mathrm{D}}(n_1) = \frac{1}{PQ}\sum_{p=1}^{P}\sum_{q=1}^{Q}\boldsymbol{\alpha}(n_1)\boldsymbol{\alpha}^H(n_1). \tag{19}$$

Consider a recursion form of $\overline{\mathbf{R}}_{2\mathrm{D}}^{n^{'}}(n_1)$ on each segment, given by:

$$\begin{aligned}\overline{\mathbf{R}}_{2\mathrm{D}}^{n^{'}}(n_1) &= \omega\overline{\mathbf{R}}_{2\mathrm{D}}^{n^{'}-1}(n_1) \\ &+ \frac{1}{PQ}\sum_{p=1}^{P}\sum_{q=1}^{Q}\mathbf{r}_{2\mathrm{D}(p,q)}^{n^{'}}(n_1)\mathbf{r}_{2\mathrm{D}(p,q)}^{n^{'}H}(n_1)\end{aligned} \tag{20}$$

where ω is the forgetting factor.

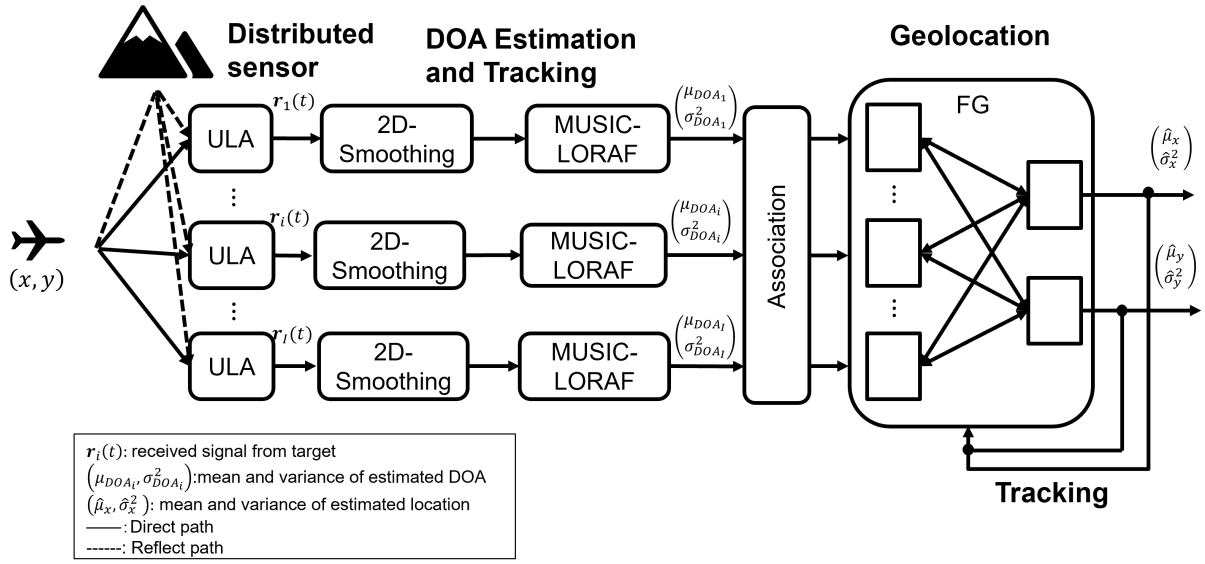

FIGURE 2. REC-SaFG framework for DoA estimation and geolocation

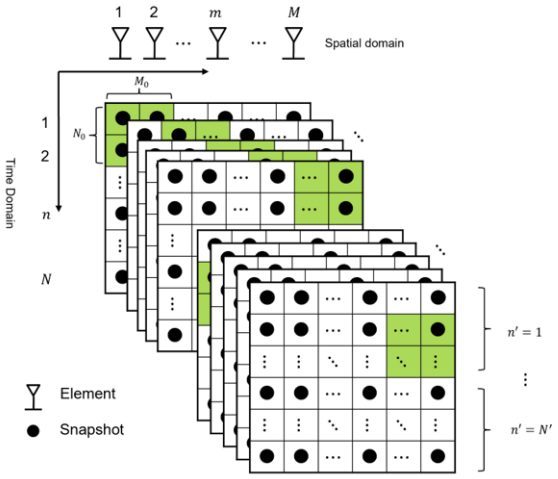

FIGURE 3. Recursive 2D smoothing

Next, define a simultaneous iteration in the LORAF algorithm by introducing a recursive vector $\mathbf{U}$ to track the subspace, given by:

$$Z^{n'}(n_1) = \overline{\mathbf{R}}^{n'}_{2\mathrm{D}}(n_1)\mathbf{U}^{n'-1}(n_1), \tag{21a}$$

$$Z^{n'}(n_1) = \mathbf{U}^{n'}(n_1)\mathbf{V}^{n'}(n_1) \tag{21b}$$

where $\mathbf{U}^{n'}(n_1)$ and $\mathbf{V}^{n'}(n_1)$ are the components of QR-decomposition. It should be noted that once iteration is over, the matrix $\mathbf{U}^{n'}(n_1)$ and $\mathbf{V}^{n'}(n_1)$ converge toward the principal eigenvectors and the corresponding eigenvalues. Hence, the approximation of EVD of the 2D smoothed covariance matrix can be expressed as:

$$\hat{\overline{\mathbf{R}}}^{n'}_{2\mathrm{D}}(n_1) = \mathbf{U}^{n'}(n_1)\mathbf{V}^{n'}(n_1)\mathbf{U}^{n'-1}(n_1)^H. \tag{22}$$

After completing the iteration process, the subspace-based methods can be employed to estimate the DoAs using the converged eigenvector. It is important to recognize the trade-off between the number of iterations and the estimation accuracy: as the number of iterations increases, so does the accuracy of the estimation. This trade-off is determined by the signal-to-noise ratio (SNR), the variation speed, and the required level of the estimation accuracy.

B. DISTANCE AND ANGLE BASED ASSOCIATION TECHNIQUE

In [5], we have introduced an association technique for multi-target identification that uses both the TOA and the DoA measurements. However, employing TOA requires maintaining system synchronization between targets and sensors. This implies that not only the TOA but also the time-of-departure (TOD) must be known to the fusion center. To improve robustness, we propose a novel association method that utilizes the DoA and the TDoA and a manually established dummy TOD to identify the direct path in this paper, as shown in Fig. 4. Note that the dummy TOD can be set arbitrarily since only the intersection clusters need to be identified rather than the accurate positions of the target.

Based on the DoA and the relative distance calculated by the time difference between the dummy TOD and the TOA, the location of the dummy target from *i*-th sensor is given by:

$$\begin{bmatrix} \hat{x}_{i,dummy} \\ \hat{y}_{i,dummy} \end{bmatrix} = \begin{bmatrix} c \times \left(t_i - t_0^{'}\right) \times \cos\phi_i \pm X_i \\ c \times \left(t_i - t_0^{'}\right) \times \sin\phi_i \pm Y_i \end{bmatrix} \tag{23}$$

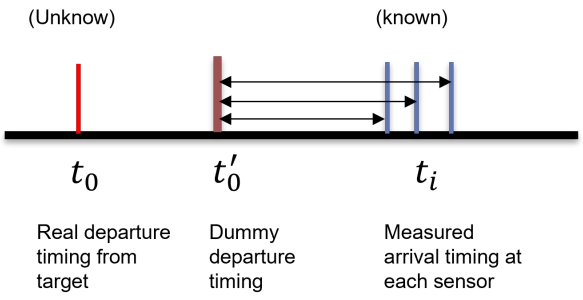

(a) Dummy TOD setting

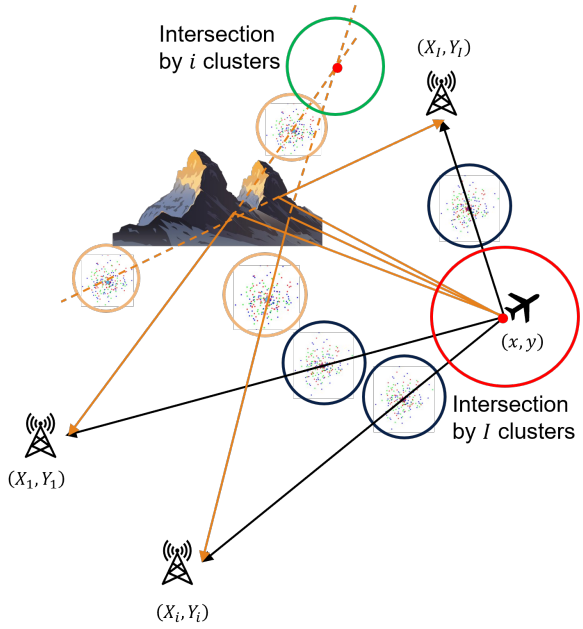

(b) Majority vote for identifying the direct path

FIGURE 4. Distance and angle-based association technique

where c is the speed of light, t_i is the measured signal arriving time at i-th sensor and $t_0^{'}$ is the dummy signal departure time manually set since the real departure time t_0 is unknown to the system. Note that DoA ϕ_i denotes the DoA of the direct path or the reflect path. According to the trigonometry relationship, all clusters related to the direct path or the reflect path are found.

The whole association can be organized as following steps:

- Step 1: Setting a dummy timing of the TOD $t_0^{'}$ manually;
- Step 2: Calculate the dummy target location based on the angle and the time difference between the TOA and the dummy TOD;
- Step 3: Extend the dummy target location along each angle;
- Step 4: Use majority vote to find the intersection cluster by I clusters to identify the direct path;
- Step 5: Label all I clusters which each can be extended to the major intersection;
- Step 6: Label the DoA range of each cluster with the direct path.

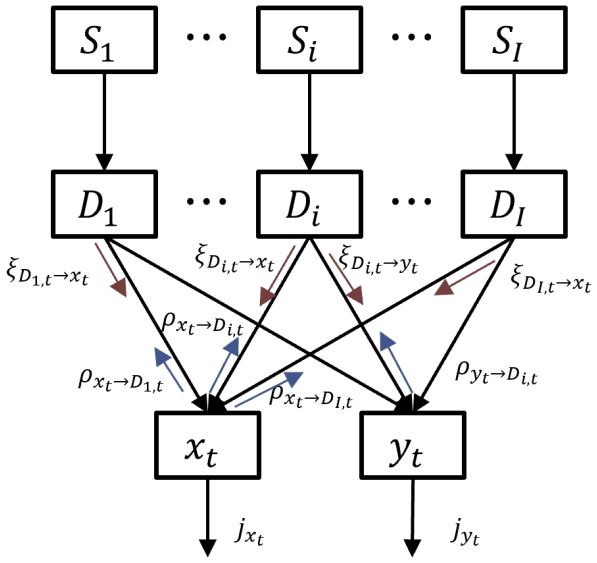

FIGURE 5. Proposed FG-GE for geolocation

It should be noted that this technique is the pre-procedure to identify the direct path. The DoA range of each direct path is roughly estimated by the trigonometric function. This roughly estimated DoA range cannot be used for geolocation. Other clustering methods, such as k-means [33], can also be used.

C. UNIFIED FG-GE-TR FOR GEOLOCATION AND TRACKING

1) FG-GE for geolocation

An important prerequisite for the FG is that all messages that are exchanged and updated obey a Gaussian distribution. Therefore, to satisfy such prerequisite, the first-order TS expansion [16] is used to approximate the nonlinear integration relationship between the true DoA and the target location, defined in (6), given by:

$$\phi_t \approx \eta_1 x + \eta_2 y + \eta \tag{24}$$

where η_1, η_2 and η_3 are constants, given by:

$$\eta_1 = \frac{Y - y_{t|t-1}}{(X - x_{t|t-1})^2 + (Y - y_{t|t-1})^2}, \tag{25}$$

$$\eta_2 = \frac{-(X - x_{t|t-1})}{(X - x_{t|t-1})^2 + (Y - y_{t|t-1})^2}, \tag{26}$$

$$\begin{aligned}\eta_3 =& \frac{(X - x_{t|t-1}) \cdot y_{t|t-1} - (Y - y_{t|t-1}) \cdot x_{t|t-1}}{(X - x_{t|t-1})^2 + (Y - y_{t|t-1})^2} \\ &+ \arctan\left(\frac{Y - y_{t|t-1}}{X - x_{t|t-1}}\right).\end{aligned} \tag{27}$$

From (24), we can derive the location of the target, express as:

$$x_t = \frac{\phi_t - \eta_2 y - \eta_3}{\eta_1}, \tag{28a}$$

$$y_t = \frac{\phi_t - \eta_1 x - \eta_3}{\eta_2}. \tag{28b}$$

Based on (28) and considering all distributed sensors, the FG-GE is constructed for geolocation, as shown in Fig. 5. In the FG-GE, the function node S_i is the measurement node for the DoA estimation by the recursive subspace-based technique in Section III-A. The estimated DoAs are sent to the next function node D_i, the compression node, to calculate the mean and the variance, i.e., $(m_{\phi_i}, \sigma^2_{\phi_i})$. The mean and the variance of the DoAs are sent to the estimation node x_t and y_t, for iteration. Let $\xi_{D_{i,t}\to x_t}$ and $\xi_{D_{i,t}\to y_t}$ denote the downward message from the compression node D_i to the estimation nodes x_t and y_t, respectively. The message $\rho_{x_t\to D_{i,t}}$ and $\rho_{y_t\to D_{i,t}}$ are the upward message from the estimation node to the compression node. The iteration process is given by:

- Downward message flow:

$$m_{\xi_{D_{i,t}\to x_t}} = \frac{1}{\eta_1} m_{\phi_i} - \frac{\eta_2}{\eta_1} m_{\rho_{y_t\to D_{i,t}}} - \frac{\eta_3}{\eta_1}, \tag{29}$$

$$\sigma^2_{\xi_{D_{i,t}\to x_t}} = \frac{1}{\eta_1^2}\sigma^2_{\phi_i} + \left(\frac{\eta_2}{\eta_1}\right)^2 \sigma^2_{\rho_{y_t\to D_{i,t}}}, \tag{30}$$

$$m_{\xi_{D_{i,t}\to y_t}} = \frac{1}{\eta_2} m_{\phi_i} - \frac{\eta_1}{\eta_2} m_{\rho_{x_t\to D_{i,t}}} - \frac{\eta_3}{\eta_2}, \tag{31}$$

$$\sigma^2_{\xi_{D_{i,t}\to y_t}} = \frac{1}{\eta_2^2}\sigma^2_{\phi_i} + \left(\frac{\eta_1}{\eta_2}\right)^2 \sigma^2_{\rho_{x_t\to D_{i,t}}}. \tag{32}$$

- Upward message flow:

$$\frac{1}{\sigma^2_{x_t\to D_{i,t}}} = \sum_{k=1,k\neq i}^{I} \frac{1}{\sigma^2_{\xi_{D_{k,t}\to x_t}}}, \tag{33}$$

$$m_{\rho_{x_t\to D_{i,t}}} = \sigma^2_{x_t\to D_{i,t}} \cdot \sum_{k=1,k\neq i}^{I} \frac{m_{\xi_{D_{k,t}\to x_t}}}{\sigma^2_{\xi_{D_{k,t}\to x_t}}}, \tag{34}$$

$$\frac{1}{\sigma^2_{y_t\to D_{i,t}}} = \sum_{k=1,k\neq i}^{I} \frac{1}{\sigma^2_{\xi_{D_{k,t}\to y_t}}}, \tag{35}$$

$$m_{\rho_{y_t\to D_{i,t}}} = \sigma^2_{y_t\to D_{i,t}} \cdot \sum_{k=1,k\neq i}^{I} \frac{m_{\xi_{D_{k,t}\to y_t}}}{\sigma^2_{\xi_{D_{k,t}\to y_t}}}. \tag{36}$$

The iteration process ends either when the estimates are converged or when the maximum iteration time is reached. The final output $(m_{j_{x_t}}, m_{j_{y_t}})$ from the converged estimates is the target's location, given by:

$$\frac{1}{\sigma^2_{j_{x_t}}} = \sum_{k=1}^{I} \frac{1}{\sigma^2_{\xi_{D_{k,t}\to x_t}}}, \tag{37}$$

$$\frac{1}{\sigma^2_{j_{y_t}}} = \sum_{k=1}^{I} \frac{1}{\sigma^2_{\xi_{D_{k,t}\to y_t}}}, \tag{38}$$

$$m_{j_{x_t}} = \sigma^2_{j_{x_t}} \cdot \sum_{k=1}^{I} \frac{m_{\xi_{D_{k,t}\to x_t}}}{\sigma^2_{\xi_{D_{k,t}\to x_t}}}, \tag{39}$$

$$m_{j_{y_t}} = \sigma^2_{j_{y_t}} \cdot \sum_{k=1}^{I} \frac{m_{\xi_{D_{k,t}\to y_t}}}{\sigma^2_{\xi_{D_{k,t}\to y_t}}}. \tag{40}$$

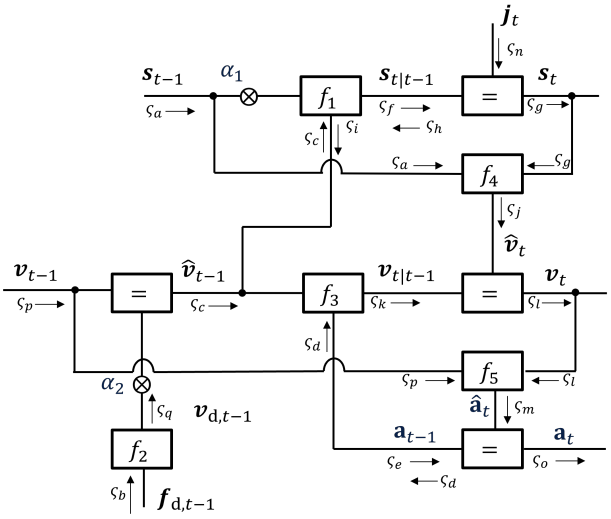

FIGURE 6. FG-GE-TR for tracking

The final output, denoted as $(m_{j_{x_t}}, m_{j_{y_t}})$, of the FG-GE serves as the observation state to refine the predicted state in the tracking phase. However, the variance $(\sigma^2_{j_{x_t}}, \sigma^2_{j_{y_t}})$ cannot be used as observation noise in accordance with the definition provided in (12). Instead, the observation noise is determined by the smallest value of σ_j^2, which is computed using the CRLB, as detailed in the Appendix.

2) FG-GE-TR for tracking

In this subsection, the tracking phase is detailed, including the state prediction, the state update, and the gradient update. The FG for tracking is constructed, as shown in Fig. 6. To predict the next state of the target, the proposed estimator aims to find the maximum posterior probability as in [16], given by:

$$p(\mathbf{s}_t, \mathbf{v}_t, \mathbf{a}_t|\mathbf{j}_{1:t}) = \sum_{\sim\mathbf{s}_t, \sim\mathbf{v}_t, \sim\mathbf{a}_t} p(\mathbf{s}_{1:t}, \mathbf{v}_{1:t}, \mathbf{a}_{1:t}|\mathbf{j}_{1:t}) \tag{41}$$

where the subscript $1{:}t$ denotes the time series and $\sim$ is the exclusion operation. As in [5], [16], based on the Bayes's theorem, (41) can be recursively updated from the previous state, given by:

$$\begin{aligned} &p(\mathbf{s}_{1:t}, \mathbf{v}_{1:t}, \mathbf{a}_{1:t}|\mathbf{j}_{1:t}) \\ &\propto \prod_{1:t} p(\mathbf{s}_t|\mathbf{s}_{t-1}, \mathbf{v}_{t-1}) p(\mathbf{v}_t|\mathbf{v}_{t-1}, \mathbf{a}_{t-1}) p(\mathbf{a}_t|\mathbf{a}_{t-1}) p(\mathbf{j}_t|\mathbf{s}_t) \end{aligned} \tag{42}$$

where $\prod$ denotes iteration steps from 1 to t. Based on (42), the whole tracking phase can be summarized as three steps:

- Step 1: State prediction
  As shown in Fig. 6, the prediction state $\mathbf{s}_{t|t-1}$ is obtained from the previous state, which is the output of FG-GE-TR at the time $t-1$. The message flow of $\mathbf{s}_{t|t-1}$ in the FG is given by:

$$\begin{aligned} &\varsigma_f(\mathbf{s}_{t|t-1}) \\ &= \sum_{\mathbf{s}_{t-1}} \sum_{\hat{\mathbf{v}}_{t-1}} f_1(\mathbf{s}_t|\mathbf{s}_{t-1}, \hat{\mathbf{v}}_{t-1}) \varsigma_a(\mathbf{s}_{t-1}) \varsigma_c(\hat{\mathbf{v}}_{t-1}) \end{aligned} \tag{43}$$

where the message flow $\varsigma_a(\mathbf{s}_{t-1})$ and $\varsigma_c(\hat{\mathbf{v}}_{t-1})$ are the output of the previous state, $f_1(\mathbf{s}_t|\mathbf{s}_{t-1}, \hat{\mathbf{v}}_{t-1})$ is the state prediction function with the forgetting factor α_1, given by:

$$f_1(\mathbf{s}_t|\mathbf{s}_{t-1}, \hat{\mathbf{v}}_{t-1}) = \alpha_1 \cdot \mathbf{s}_{t-1} + \hat{\mathbf{v}}_{t-1} \tag{44}$$

It should be noted that our focus is on the tracking of an aircraft, which inherently involves high velocity and long-range detection during the tracking phase. Despite the DoA output from the recursive subspace-based techniques having minimal estimation errors, the geolocation error turns into magnificent due to the extensive distances. Therefore, to balance the effect between the large state difference due to the long range and the velocity change, the forgetting factor α_1 is introduced in the prediction function.

- Step 2: State update
To obtain the current state $\mathbf{s}_t$, the FG-GE output $\mathbf{j}_t$ is used as an observation to refine the prediction state $\mathbf{s}_t|\mathbf{s}_{t-1}$. $\mathbf{s}_t$ is thereby given as:

$$\varsigma_g(\mathbf{s}_t) = \varsigma_f(\mathbf{s}_t|\mathbf{s}_{t-1})\varsigma_n(\mathbf{j}_t) \tag{45}$$

- Step 3: Gradient update
In this step, two gradient vectors, $\mathbf{v}_t$ and $\mathbf{a}_t$, are updated in each tracking state. The velocity is obtained from the Doppler frequency which is the output of the recursive subspace-based techniques. The velocity is thereby given by:

$$\varsigma_q(\mathbf{v}_{\mathrm{d},t-1}) = \sum_{\mathbf{f}_{\mathrm{d},t-1}} f_2(\mathbf{f}_{\mathrm{d},t-1})\varsigma_b(\mathbf{f}_{\mathrm{d},t-1}) \tag{46}$$

where the function $f_2(\mathbf{f}_{\mathrm{d},t-1})$ is given by:

$$f_2(\mathbf{f}_{\mathrm{d},t-1}) = \frac{\mathbf{f}_{\mathrm{D}} \cdot \lambda}{\cos\hat{\phi}} \tag{47}$$

with $\hat{\phi}$ the DoA output from the recursive subspace-based techniques. The velocity can be updated using a correction term $\hat{\mathbf{v}}_t$ to refine the predicted velocity $\mathbf{v}_{t|t-1}$ that is determined by the previous velocity vector $\hat{\mathbf{v}}_{t-1}$ and the acceleration vector $\mathbf{a}_{t-1}$. Therefore, the current velocity $\mathbf{v}_t$ is given by:

$$\varsigma_l(\mathbf{v}_t) = \varsigma_j(\hat{\mathbf{v}}_t)\varsigma_k(\mathbf{v}_{t|t-1}) \tag{48}$$

where the message flow $\varsigma_j(\hat{\mathbf{v}}_t)$ is obtained by letting the state difference between two adjacent locations divided by time unit, given by:

$$\varsigma_j(\hat{\mathbf{v}}_t) = \sum_{\mathbf{s}_{t-1}}\sum_{\mathbf{s}_t} f_4(\hat{\mathbf{v}}_t|\mathbf{s}_t, \mathbf{s}_{t-1})\varsigma_a(\mathbf{s}_{t-1})\varsigma_g(\mathbf{s}_t) \tag{49}$$

where the function $f_4(\hat{\mathbf{v}}_t|\mathbf{s}_t, \mathbf{s}_{t-1})$ is given by:

$$f_4(\hat{\mathbf{v}}_t|\mathbf{s}_t, \mathbf{s}_{t-1}) = \mathbf{s}_t - \mathbf{s}_{t-1} \tag{50}$$

The message flow $\varsigma_k(\mathbf{v}_{t|t-1})$ is calculated from the previous velocity plus the product of acceleration and unit time, given by:

$$\varsigma_k(\mathbf{v}_{t|t-1}) = \sum_{\hat{\mathbf{v}}_{t-1}}\sum_{\mathbf{a}_{t-1}} f_3(\mathbf{v}_{t|t-1}|\hat{\mathbf{v}}_{t-1}, \mathbf{a}_{t-1})\varsigma_c(\hat{\mathbf{v}}_{t-1})\varsigma_D(\mathbf{a}_{t-1}) \tag{51}$$

where the function $f_3(\mathbf{v}_{t|t-1}|\hat{\mathbf{v}}_{t-1}, \mathbf{a}_{t-1})$ is given by:

$$f_3(\mathbf{v}_{t|t-1}|\hat{\mathbf{v}}_{t-1}, \mathbf{a}_{t-1}) = \hat{\mathbf{v}}_{t-1} + \mathbf{a}_{t-1} \tag{52}$$

The velocity vector $\hat{\mathbf{v}}_{t-1}$ is the combination of the previous velocity state $\mathbf{v}_{t-1}$ of the FG-GE-TR and the input velocity $\mathbf{v}_{d,t-1}$ from the recursive MUSIC-LORAF, given by:

$$\hat{\mathbf{v}}_{t-1} = \alpha_2 \cdot \mathbf{v}_{\mathrm{d},t-1} + \mathbf{v}_{t-1} \tag{53}$$

It should be noted that the coefficient α_2 acts as a forgetting factor, helping to mitigate the impact of the high mobility. This is because the input velocity $\mathbf{v}_{\mathrm{d},t-1}$, derived from the recursive MUSIC-LORAF at each time step, lacks memory of the previous state. In high mobility scenarios, abrupt changes in the value of $\mathbf{v}_{\mathrm{d},t-1}$ can compromise the stability of the tracking phase.
To update the acceleration component, a correction term $\hat{\mathbf{a}}_t$ is introduced, which is calculated by the subtract of two adjacent velocity divided by the unit time, given by:

$$\varsigma_m(\hat{\mathbf{a}}_t) = \sum_{\mathbf{v}_{t-1}}\sum_{\mathbf{v}_t} f_5(\hat{\mathbf{a}}_t)\varsigma_c(\mathbf{v}_{t-1})\varsigma_l(\mathbf{v}_t) \tag{54}$$

where the function $f_5(\hat{\mathbf{a}}_t)$ is given by:

$$f_5(\hat{\mathbf{a}}_t) = \mathbf{v}_t - \mathbf{v}_{t-1} \tag{55}$$

Thereby, the updated acceleration is given by:

$$\varsigma_o(\mathbf{a}_t) = \varsigma_e(\mathbf{a}_{t-1})\varsigma_m(\hat{\mathbf{a}}_t) \tag{56}$$

IV. RESULTS AND DISCUSSION

Numerical simulation results are provided to illustrate the performance of the proposed Rec-SaFG framework. The DoA estimation by the recursive subspace-based technique is first evaluated. Then the accuracy of the geolocation and the tracking, that is, FG-GE and FG-GE-TR, is analyzed as well.

A. DOA ESTIMATION AND TRACKING BY RECURSIVE MUSIC-LORAF

Similar to [23], [24], the signal model in terms of two coherent paths is used, one direct path and one reflect path with empirical nonstationarity. The parameters setting for the DoA estimation by recursive MUSIC-LORAF are summarized in the TABLE. 1.

The accuracy of the DoA estimation is evaluated by calculating the root mean square error (RMSE), defined as:

$$RMSE_{\mathrm{DoA}} = \sqrt{\sum_{k=1}^{K} \frac{\hat{\phi}_{\mathrm{D},k}^{i} - \phi_{\mathrm{D}}^{i}}{K}} \tag{57}$$

TABLE 1. Parameters setting of DoA estimation by recursive MUSIC-LORAF

Symbol	Quantity	Value
$\beta_{\mathrm{D}}; \beta_{\mathrm{R}}$	amplitude of direct path and reflect path	1
M	number of elements of the array	8
N	snapshot	100
$N^{'}$	number of segments of snapshot	10
$\triangle T$	sampling interval	1/1000 s
$f_{d_{\mathrm{D}}}$	Doppler frequency of direct path	10 Hz
$f_{d_{\mathrm{R}}}$	Doppler frequency of reflect path	7 Hz
d	element spacing	1.5 m
λ	wave length	3
M_0	number of element in each sub-array	3
N_0	number of snapshot in each sub-snapshot	50
P	number of subarrays	6
Q	number of subsnapshots	51
I	number of sensors	3
(X_1, Y_1)	position of sensor 1	$(0, -1)$ km
(X_2, Y_2)	position of sensor 2	$(8, 10)$ km
(X_3, Y_3)	position of sensor 3	$(15, -2)$ km

where K is the times of Monte Carlo simulation. The RMSE of the DoA of the reflect path can be calculated in the same way. The performance of the DoA estimation versus different SNR is shown in Fig. 7. According to the simulation results, the proposed recursive MUSIC-LORAF can decorrelate the two coherent paths and achieve high DoA estimation accuracy for the direct path and the reflect path. Although the machine learning-based techniques, as in [25], [26], can achieve higher accuracy in the DoA estimation, the proposed recursive subspace-based technique provides sufficiently accurate DoA estimates with greater simplicity and computational efficiency for the FG-GE. Due to the fact that the estimation performance is also dependent on the recursive time, the convergence performance is evaluated through the iterative steps ($n^{'}$-th segment of all $N^{'}$ segments) with SNR = 20 dB, as shown in Fig. 8. Clearly, the accuracy of the estimation improves with an increase in the recursion time. The analysis of convergence is crucial for balancing the accuracy of the estimation against the processing time in practical applications. The implications of this trade-off on geolocation and tracking are analyzed in the following subsection.

For the DoA tracking scenario, the trajectory of an aircraft is designed in the same way as in [24], given by:

$$x_n = x_{n-1} + a\cos\left(n \cdot \varpi\right) + \upsilon_{x,n} \tag{58a}$$

$$y_n = y_{n-1} + a\sin\left(n \cdot \varpi\right) + \upsilon_{y,n} \tag{58b}$$

where $t = \{1, 2, \cdots, 40\}$ is the measurement time, $a = 1\mathrm{km}$ is the radius of the motion, $\varpi = \frac{\pi}{50}\mathrm{rad/s}$ is the angular velocity, $\boldsymbol{\upsilon}_n = [\upsilon_{x,n}, \upsilon_{y,n}]^T$ denotes the random deviation of the trajectory from the ideal path which is Gaussian distribution $\boldsymbol{\upsilon} \sim (0, \sigma_v^2), \sigma_v = 0.32\mathrm{km/s}$. The average RMSE of the DoA tracking over the trajectory is calculated to evaluate the DoA tracking performance, given by:

$$\overline{RMSE}_{\mathrm{DoA}} = \sqrt{\sum_{t=1}^{T} \frac{\hat{\phi}_{\mathrm{D},t}^{i} - \phi_{\mathrm{D},t}^{i}}{T}} \tag{59}$$

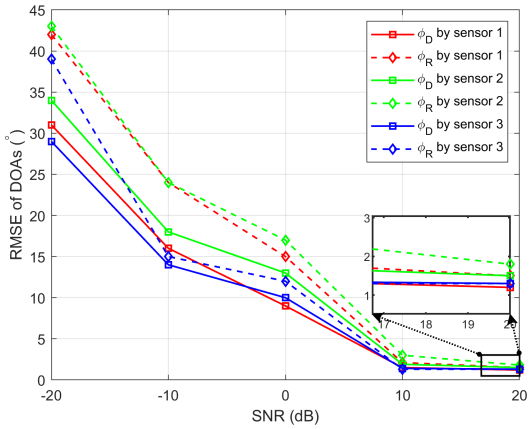

FIGURE 7. RMSE of DoA estimation vs. SNR

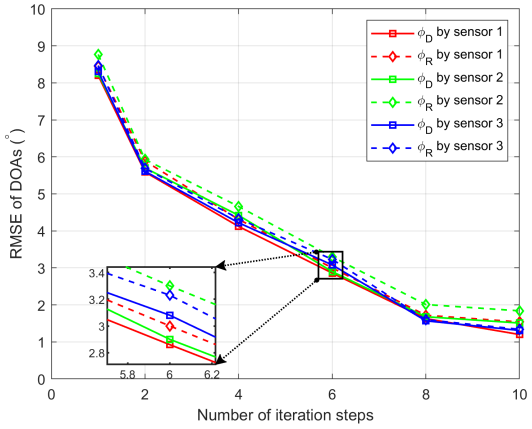

FIGURE 8. Convergence analysis of recursive MUSIC-LORAF with SNR=20 dB

where T is the trajectory time of the moving target. The average RMSE for tracking of the DoA vs. SNR is summarized in TABLE 2. The simulation results indicate that the proposed recursive MUSIC-LORAF technique is capable of achieving high accuracy in the DoA tracking scenarios.

TABLE 2. Average RMSE (°) of DoA tracking via SNR

DoA \ SNR (dB)	-20	-10	0	10	20
ϕ_{D}^{1}	35.39	19.21	12.84	4.84	2.28
ϕ_{R}^{1}	39.77	21.89	14.01	5.01	2.82
ϕ_{D}^{2}	47.11	23.47	17.30	5.39	3.10
ϕ_{R}^{2}	49.31	25.02	19.78	7.78	3.99
ϕ_{D}^{3}	36.21	21.16	15.25	5.22	2.61
ϕ_{R}^{3}	37.42	22.16	16.41	5.41	2.72

B. GEOLOCATION BY FG-GE

The position of the target is estimated by inputting the DoA of the direct path, which is determined by the recursive MUSIC-LORAF algorithm, into the FG-GE for iterative processing. It

should be noted that the FG's input must follow the Gaussian distribution. The probability density function (pdf) of the DoA message is empirically obtained by the Monte Carlo simulation. The pdf of the DoA of the direct path between the target and sensor 1 is depicted in Fig. 9. It can be easily found that the DoA estimated by the recursive MUSIC-LORAF follows the Gaussian distribution, with a mean of $14.63°$ and a variance of $0.0071°$. The pdf of the DOA of the direct path in other sensors can be achieved similarly.

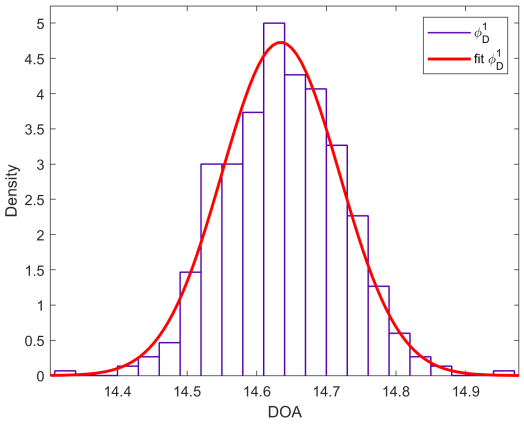

FIGURE 9. PDF of ϕ_D^1 with confidence bound 95% with SNR = 20 dB

The pdf message of the DoA from each sensor is input into the FG-GE fusion for exchanging and updating. Let the iteration times for FG-GE be 20 and the initial guess of the target be $(0, 0)$ for iteration. The convergence behavior of the FG-GE is evaluated by calculating the RMSE of estimated position, given by:

$$RMSE_{x,y} = \sqrt{\sum_{k'=1}^{K'} \frac{(\hat{x}_{k'} - x)^2 + (\hat{y}_{k'} - y)^2}{K'}} \tag{60}$$

As shown in Fig. 10(a), the position estimates of the FG-GE rapidly converge within just 5 iterations. Furthermore, as demonstrated in Fig. 10(b), the estimated target position approaches very close to the true value, even when the initial guess is significantly far away from the true position.

In the Rec-SaFG framework, the first-step approach, recursive MUSIC-LORAF, has an important effect on the second-step approach, the FG-GE. To evaluate the trade-off between the accuracy and the fast estimation process, the effect of the number of recursion steps in recursive MUSIC-LORAF on the target position estimation is evaluated. The simulation results are shown in Fig. 11. As we expected in Chapter. III, the target geolocation performance improves with an increase in recursion steps.

C. TRACKING BY FG-GE-TR

The same trajectory of the aircraft, defined in (58), is used to evaluate the performance of FG-GE-TR. The tracking perfor-

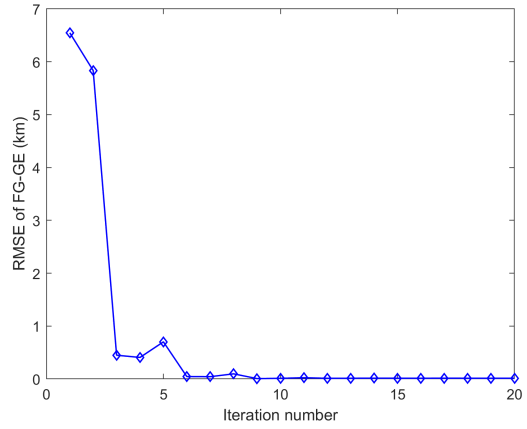

(a) RMSE of FG-GE vs. iteration number

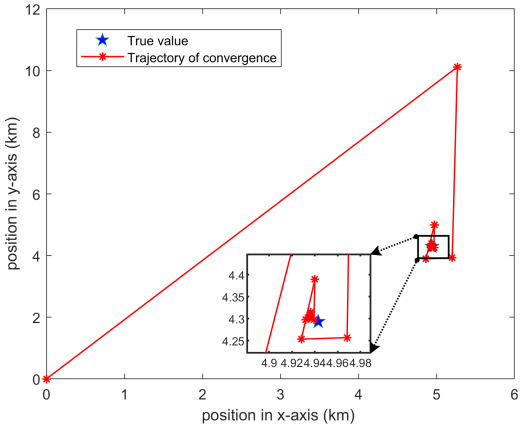

(b) Trajectory of convergence

FIGURE 10. Convergence behavior analysis of FG-GE with SNR = 20 dB

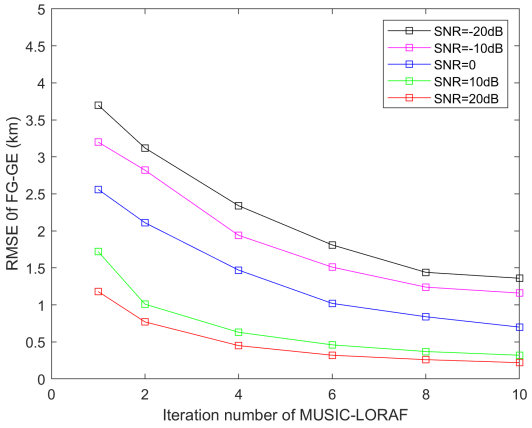

FIGURE 11. RMSE of FG-GE vs. iteration number of MUSIC-LORAF with SNR = 20 dB

mance of the proposed method, which includes an acceleration update component within the FG framework, is evaluated against a prior technique that lacks this feature, as referenced in [5]. The geolocation and trajectory tracking enabled by the FG-GE and the FG-GE-TR are shown in Fig. 12. The average RMSE for the tracking phase is calculated for comparison. The simulation results reveal that the FG-GE-TR achieves superior tracking accuracy for fast-moving targets when the acceleration component is incorporated. This enhancement is also attributed to the acceleration being updated at each iteration, helping to track the velocity and minimizing the cumulative error in the velocity update process.

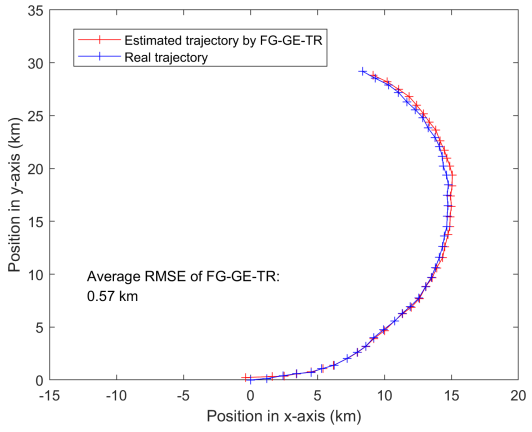

(a) Without acceleration

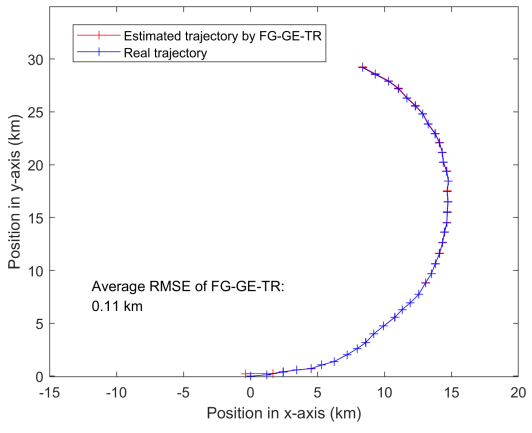

(b) With acceleration

FIGURE 12. **Trajectory tracking by FG-GE-TR with SNR=20 dB**

D. OPTIMAL FORGETTING FACTOR SELECTION

As discussed in Chapter III, in the scenarios involving the high mobility tracking, forgetting factors within the FG-GE-TR play crucial roles in improving the tracking performance. This significance stems from the fact that the forgetting factors largely depend on the target's velocity. Our goal is to empirically determine the optimal forgetting factor for different velocity scenarios. First, we set the forgetting factors

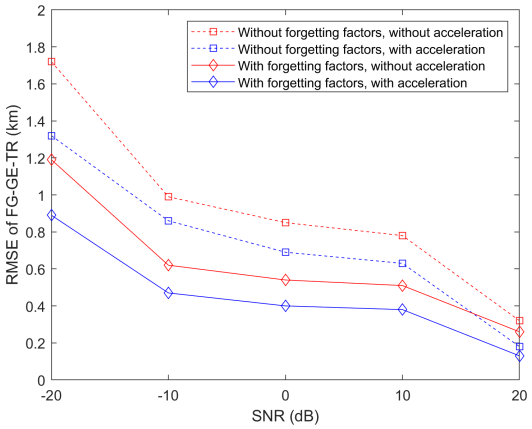

FIGURE 13. **RMSE of tracking vs. SNR**

at $\alpha_1 = \alpha_2 = 0.95$ to demonstrate the improvement of the forgetting factor in the FG-GE-TR framework. The tracking accuracy, as shown in Fig. 13, shows a clear improvement in both the acceleration and the non-acceleration cases upon incorporating forgetting factors. This improvement is attributed to the forgetting factors' ability to balance the influence of the previous states and the new observations, thereby enhancing the prediction of the state in cases of the high mobility.

Next, to evaluate the effect of the forgetting factors on the tracking part, the average speed is used and given by:

$$\overline{v} = \sum_{t=1}^{T} \frac{\sqrt{(x_t - x_{t-1})^2 + (y_t - y_{t-1})^2}}{T \cdot \triangle t} \tag{61}$$

The simulation results are shown in Fig. 14. Note that the optimal forgetting factors are empirically identified by minimizing the RMSE of FG-GE-TR in various speed scenarios. The simulation results indicate a trend where higher speeds correlate with lower optimal forgetting factors. This trend arises because, in cases of high-speed movement, the influence of the previous state on the current state diminishes. Consequently, the current observations are of greater significance in predicting the state.

Furthermore, the two forgetting factors, α_1 and α_2, serve different purposes. α_1 is designed to mediate the impact between the position and the velocity states. Given the longer measurement range, the difference between two consecutive positions tends to be greater than that in the velocity state. Hence, the forgetting factor α_1 should place greater emphasis on the position state. Its value should not be excessively reduced, even with increasing speed, as illustrated in Fig. 14(a).

The forgetting factor α_2 aims to balance the two velocities: (1) estimated from the recursive MUSIC-LORAF algorithm and (2) output from the FG-GE-TR. The velocity from the recursive MUSIC-LORAF, serving as the observation state without historical memory, can introduce instability to the overall FG structure, particularly in the high mobility sce-

narios. To maintain the stability, α_2 is adjusted downward to diminish the influence of the observation state's velocity. This adjustment allows the previous velocity state of the FG-GE-TR to provide a greater influence on the prediction of the subsequent state's velocity, as shown in Fig. 14(b).

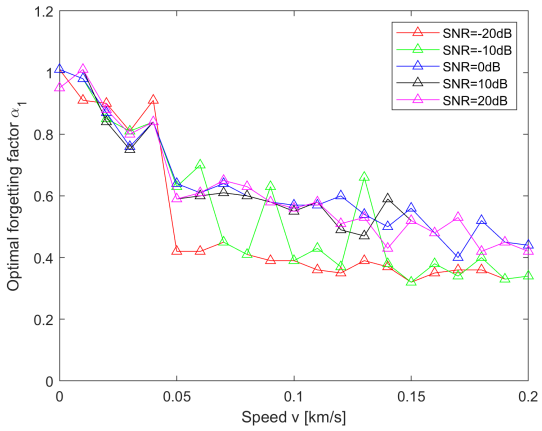

(a) Tendency of α_1

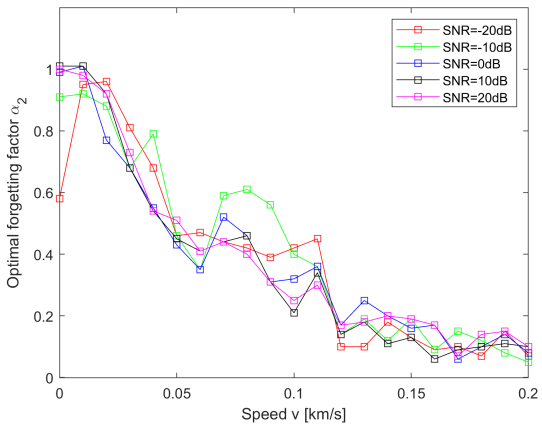

(b) Tendency of α_2

FIGURE 14. Optimal forgetting factor vs. speed with SNR=20 dB

V. CONCLUSION

This paper has proposed REC-SaFG, a recursive subspace and factor graph framework for DoA estimation and geolocation of a fast-moving target. A generic received signal model was first introduced for the case of a fast-moving target with multiple coherent propagation paths. It has been shown that the proposed 2D smoothing solution is effective for decorrelating the coherent signals in the presence of empirical nonstationarity due to the insufficient sample size compared to the target moving speeds. A subspace algorithm combined with a recursive subspace tracking algorithm, MUSIC-LORAF, has been used for DoA estimation and tracking iteratively. Moreover, it has been shown that the proposed framework can combine geolocation and tracking into one single factor graph. In the unified FG, the velocity difference in the present and past states is taken into account, resulting in tracking performance enhancement without sacrificing the tracking stability. Extension of the proposed technique to multiple target cases is left for future research.

VI. APPENDIX

A. LORAF-BASED SUBSPACE TRACKING OF 2D SMOOTHED COVARIANCE MATRIX

The EVD approximation of the 2D smoothed covariance matrix can be used to track the corresponding eigenvectors and eigenvalues related to the signal subspace. Substituting (20) into (21a), we can rewrite (21a) as:

$$Z^{n^{'}}(n_1) = \omega \overline{\mathbf{R}}_{2\mathrm{D}}^{n^{'}-1}(n_1)\mathbf{U}^{n^{'}-1}(n_1) + \mathbf{r}_{2\mathrm{D}}^{n^{'}}(n_1)\mathbf{h}^{n^{'}}(n_1)^H \quad (62)$$

where

$$\mathbf{h}^{n^{'}}(n_1) = \mathbf{U}^{n^{'}-1}(n_1)^H \mathbf{r}_{2\mathrm{D}}^{n^{'}}(n_1). \quad (63)$$

Furthermore, the approximation $\hat{\overline{\mathbf{R}}}_{2\mathrm{D}}^{n^{'}}(n_1)$ is used to replace the true value $\overline{\mathbf{R}}_{2\mathrm{D}}^{n^{'}}(n_1)$. Then (62) can be derived as:

$$\begin{aligned} Z^{n^{'}}(n_1) &= \omega Z^{n^{'}-1}(n_1)\boldsymbol{\Theta}^{n^{'}}(n_1) \\ &\quad + \mathbf{r}_{2\mathrm{D}}^{n^{'}}(n_1)\mathbf{r}_{2\mathrm{D}}^{n^{'}}(n_1)^H \mathbf{U}^{n^{'}-1}(n_1) \end{aligned} \quad (64)$$

where $\boldsymbol{\Theta}^{n^{'}}(n_1) = \mathbf{U}^{n^{'}-1}(n_1)^H \mathbf{U}^{n^{'}-1}(n_1)$ is the rotation matrix. The whole subspace tracking algorithm is summarized in Algorithm 1.

Algorithm 1 LORAF-based subspace tracking of 2D smoothed covariance matrix

Initialization: $\mathbf{U}^1(n_1) = \begin{bmatrix} \mathbf{I} \\ 0 \end{bmatrix}_{\frac{MN}{N^{'}} \times 2}$; $\boldsymbol{\Theta}^1(n_1) = \mathbf{I}_{2\times 2}$;

$\omega : 0 \le \omega \le 1$; $N^{'}$: Segments; rank: 2

Require: $\mathbf{r}_{2\mathrm{D}}^{n^{'}}(n_1)$

Subspace tracking

for $n^{'} \leftarrow 1$ to $N^{'}$ **do**,

$\mathbf{h}^{n^{'}}(n_1)_{2\times 1} = \mathbf{U}^{n^{'}-1}(n_1)^H \mathbf{r}_{2\mathrm{D}}^{n^{'}}(n_1)$

$Z^{n^{'}}(n_1)_{\frac{MN}{N^{'}}\times 2} = \omega Z^{n^{'}-1}(n_1)\boldsymbol{\Theta}^{n^{'}-1}(n_1) + \mathbf{r}_{2\mathrm{D}}^{n^{'}}(n_1)\mathbf{h}^{n^{'}}(n_1)$

$Z^{n^{'}}(n_1) = \mathbf{U}^{n^{'}}(n_1)_{\frac{MN}{N^{'}}\times 2}\mathbf{V}^{n^{'}}(n_1)_{2\times 2}$

$\boldsymbol{\Theta}^{n^{'}}(n_1) = \mathbf{U}^{n^{'}-1}(n_1)^H \mathbf{U}^{n^{'}}(n_1)$

end for

Ensure: $\mathbf{U}^{n^{'}}(n_1)$

B. DERIVATION OF POSTERIOR PROBABILITY

According to the Bayes's theorem, (41) can be further expressed as:

$$\begin{aligned} &p(\mathbf{s}_{1:t}, \mathbf{v}_{1:t}, \mathbf{a}_{1:t} | \mathbf{j}_{1:t}) \\ &= \frac{p(\mathbf{j}_t | \mathbf{s}_{1:t}, \mathbf{v}_{1:t}, \mathbf{a}_{1:t}, \mathbf{j}_{1:t-1}) p(\mathbf{s}_{1:t}, \mathbf{v}_{1:t}, \mathbf{a}_{1:t}, \mathbf{j}_{1:t-1})}{p(j_{1:t})} \end{aligned} \quad (65)$$

Due to the fact that $\mathbf{j}_t$ only depends on $\mathbf{s}_t$, the term $p(\mathbf{j}_t|\mathbf{s}_{1:t},\mathbf{v}_{1:t},\mathbf{a}_{1:t},\mathbf{j}_{1:t-1}) = p(\mathbf{j}_t|\mathbf{s}_t)$. The probability $p(j_{1:t})$ is constant. Therefore, (65) can be further expressed as:

$$p(\mathbf{s}_{1:t},\mathbf{v}_{1:t},\mathbf{a}_{1:t}|\mathbf{j}_{1:t}) \propto p(\mathbf{j}_t|\mathbf{s}_t)p(\mathbf{s}_{1:t},\mathbf{v}_{1:t},\mathbf{a}_{1:t},\mathbf{j}_{1:t-1}) \tag{66}$$

The joint probability $p(\mathbf{s}_{1:t},\mathbf{v}_{1:t},\mathbf{a}_{1:t},\mathbf{j}_{1:t-1})$ can be further derived as:

$$\begin{aligned} &p(\mathbf{s}_{1:t},\mathbf{v}_{1:t},\mathbf{a}_{1:t},\mathbf{j}_{1:t-1}) \\ =&p(\mathbf{s}_t|\mathbf{s}_{t-1},\mathbf{v}_{t-1})p(\mathbf{v}_t|\mathbf{v}_{t-1},\mathbf{a}_{t-1})p(\mathbf{a}_t|\mathbf{a}_{t-1}) \\ &\cdot p(\mathbf{s}_{1:t-1},\mathbf{v}_{1:t-1}|\mathbf{j}_{1:t-1})p(\mathbf{j}_{1:t-1}) \end{aligned} \tag{67}$$

where the term $p(\mathbf{j}_{1:t-1})$ is constant, v_t is determined by v_{t-1} and a_{t-1}, a_t is determined by a_{t-1}. therefore, (67) is further given by:

$$\begin{aligned} &p(\mathbf{s}_{1:t},\mathbf{v}_{1:t},\mathbf{a}_{1:t},\mathbf{j}_{1:t-1}) \\ &\propto p(\mathbf{s}_t|\mathbf{s}_{t-1},\mathbf{v}_{t-1})p(\mathbf{v}_t|\mathbf{v}_{t-1},\mathbf{a}_{t-1})p(\mathbf{a}_t|\mathbf{a}_{t-1}) \\ &\cdot p(\mathbf{s}_{1:t-1},\mathbf{v}_{1:t-1},\mathbf{a}_{1:t-1}|\mathbf{j}_{1:k-1}) \end{aligned} \tag{68}$$

Note that $p(\mathbf{s}_{1:t-1},\mathbf{v}_{1:t-1},\mathbf{a}_{1:t-1}|\mathbf{j}_{1:k-1})$ is updated recursively from the previous state. Combining (66) and (68), the posterior probability is given by:

$$\begin{aligned} &p(\mathbf{s}_{1:t},\mathbf{v}_{1:t},\mathbf{a}_{1:t}|\mathbf{j}_{1:t}) \\ &\propto \prod_{1:t} p(\mathbf{s}_t|\mathbf{s}_{t-1},\mathbf{v}_{t-1})p(\mathbf{v}_t|\mathbf{v}_{t-1},\mathbf{a}_{t-1})p(\mathbf{a}_t|\mathbf{a}_{t-1})p(\mathbf{j}_t|\mathbf{s}_t) \end{aligned} \tag{69}$$

C. CALCULATION OF THE OBSERVATION NOISE

The CRLB derivation is used to derive the smallest value of σ_z^2 to present as observation noise in FG-GE-TR. The value of σ_z^2 is derived from the DoA ϕ_{D} of the direct path obtained by the recursive MUSIC-LORAF method. Note that the sensor index is omitted for simplicity unless necessary. According to [29], the CRLB is given by

$$CRLB = trace[F^{-1}(\mathbf{s})], \tag{70}$$

where F is the Fisher information matrix (FIM). Given the pdf of the variable ϕ_{D} with K samples, the FIM is then given by

$$F(\mathbf{s}) = E\left[\left(\frac{\partial}{\partial \mathbf{s}}\ln p(\widehat{\phi}_{\mathrm{D}})\right)^2\right], \tag{71}$$

where the pdf function $p(\cdot)$ is given by

$$p(\widehat{\phi}_{\mathrm{D}}) = \prod_{k=1}^{K}\frac{1}{\sqrt{2\pi\sigma_{\phi_{\mathrm{D}}}^2}}\exp\left[-\frac{1}{2\sigma_{\phi_{\mathrm{D}}}^2}(\widehat{\phi}_{D_k}-\phi_{\mathrm{D}})^2\right]. \tag{72}$$

Next, (71) is given by

$$E\left[\left(\frac{\partial}{\partial s}\ln p(\widehat{\phi}_{\mathrm{D}})\right)^2\right] = -E\left[\frac{\partial^2}{\partial\phi_{\mathrm{D}}^2}\ln p(\widehat{\phi}_{\mathrm{D}})\right]. \tag{73}$$

According to [16],

$$\frac{\partial^2}{\partial\phi_{\mathrm{D}}^2}\ln p(\widehat{\phi}_{\mathrm{D}}) = -\frac{K}{\sigma_{\phi_{\mathrm{D}}}^2}. \tag{74}$$

Then, the FIM is further expressed as

$$\begin{aligned} F(\mathbf{s}) &= \frac{\partial\phi_{\mathrm{D}}}{\partial s}^T E\left[\left(\frac{\partial}{\partial\phi_{\mathrm{D}}}\ln p(\widehat{\phi}_{\mathrm{D}})\right)^T\left(\frac{\partial}{\partial\phi_{\mathrm{D}}}\ln p(\widehat{\phi}_{\mathrm{D}})\right)\right]\frac{\partial\phi_{\mathrm{D}}}{\partial\mathbf{s}} \\ &= \frac{\partial\phi_{\mathrm{D}}}{\partial\mathbf{s}}^T E\left[\left(\frac{\partial}{\partial\phi_{\mathrm{D}}}\ln p(\widehat{\phi}_{\mathrm{D}})\right)^2\right]\frac{\partial\phi_{\mathrm{D}}}{\partial\mathbf{s}} \\ &= \frac{\partial\phi_{\mathrm{D}}}{\partial\mathbf{s}}^T\left[\frac{K}{\sigma_{\phi_{\mathrm{D}}}^2}\right]\frac{\partial\phi_{\mathrm{D}}}{\partial\mathbf{s}}. \end{aligned} \tag{75}$$

where $\frac{\partial\phi_{\mathrm{D}}}{\partial\mathbf{s}}$ is the Jacobin matrix, which is given by

$$J = \frac{\partial\phi_{\mathrm{D}}}{\partial\mathbf{s}} = \begin{bmatrix} \frac{\partial\phi_{D_1}}{\partial x} & \frac{\partial\phi_{D_1}}{\partial y} \\ \frac{\partial\phi_{D_2}}{\partial x} & \frac{\partial\phi_{D_2}}{\partial y} \\ \vdots & \vdots \\ \frac{\partial\phi_{D_I}}{\partial x} & \frac{\partial\phi_{D_I}}{\partial y} \end{bmatrix}, \tag{76}$$

with

$$\frac{\partial\phi_{D_I}}{\partial x} = \frac{Y_i - y}{d_i^2}, \tag{77}$$

$$\frac{\partial\phi_{D_I}}{\partial y} = \frac{-(X_i - x)}{d_i^2}, \tag{78}$$

where d_i is the Euclidean distance between target and sensor i. Due to the fact that the real position is unknown to the system, the prediction state $x_{t|t-1}$ and $y_{t|t-1}$ is used to calculate the CRLB. The Jacobin matrix is thereby given by

$$J_{t|t-1} = \begin{bmatrix} \frac{Y_1 - y_{t|t-1}}{d_1^2} & \frac{-(X_1 - x_{t|t-1})}{d_1^2} \\ \frac{Y_2 - y_{t|t-1}}{d_2^2} & \frac{-(X_2 - x_{t|t-1})}{d_2^2} \\ \vdots & \vdots \\ \frac{Y_I - y_{t|t-1}}{d_I^2} & \frac{-(X_I - x_{t|t-1})}{d_I^2} \end{bmatrix}. \tag{79}$$

Finally, the CRLB is given by

$$CRLB = \{\mathrm{diag}[(J_{t|t-1}^T\sum_{\phi_{\mathrm{D}}}^{-1}J_{t|t-1})K]\}^{-1}. \tag{80}$$

D. DERIVATION OF OPTIMAL FORGETTING FACTOR

To determine the optimal forgetting factor α_1, the pdfs of the target's position and velocity are assumed to be the Gaussian distribution, $A \sim \mathcal{N}\left(\alpha_1 m_{\mathbf{s},t-1}, \alpha_1^2\sigma_{\mathbf{s},t-1}^2\right)$ and $B \sim \mathcal{N}\left(m_{\mathbf{v},t-1}, \sigma_{\mathbf{v},t-1}^2\right)$. In FG-GE-TR, the Gaussian message of position and velocity is merged and sent to the next node. Therefore, the joint pdf of position and velocity is given by:

$$C \sim \mathcal{N}\left(\frac{m_{\mathbf{s},t-1}\sigma_{\mathbf{v},t-1}^2 + m_{\mathbf{v},t-1}\alpha_1^2\sigma_{\mathbf{s},t-1}^2}{\alpha_1^2\sigma_{\mathbf{s},t-1}^2 + \sigma_{\mathbf{v},t-1}^2}, \frac{1}{\frac{1}{\alpha_1^2\sigma_{\mathbf{s},t-1}^2} + \frac{1}{\sigma_{\mathbf{v},t-1}^2}}\right) \tag{81}$$

The optimal forgetting factor α_1 can be found by minimizing the variance of the joint pdf, $\sigma^2_{C,t-1}$, given by:

$$\begin{aligned}\frac{\mathrm{d}\sigma^2_{C,t-1}}{\mathrm{d}\alpha_1} &= \frac{\mathrm{d}\left(\frac{1}{\alpha_1^2\sigma^2_{\mathbf{s},t-1}} + \frac{1}{\sigma^2_{\mathbf{v},t-1}}\right)}{\mathrm{d}\alpha_1} \\ &= \frac{2\alpha_1\sigma_{\mathbf{s},t-1}\sigma^2_{\mathbf{v},t-1}}{\left(\alpha_1^2\sigma_{\mathbf{s},t-1} + \sigma_{\mathbf{v},t-1}\right)^2}\end{aligned} \tag{82}$$

The minimum value can be achieved by letting the differential (82) equal to 0. However, this differential cannot provide a meaningful solution unless $\alpha_1 = 0$. Therefore, in this paper, the value of the forgetting factor α_1 is obtained using empirical methods. The value of the forgetting factor α_2 can be obtained in the same way.

REFERENCES

[1] T. Wild, V. Braun and H. Viswanathan, "Joint Design of Communication and Sensing for Beyond 5G and 6G Systems," *IEEE Access*, vol. 9, pp. 30845-30857, 2021.
[2] A. Boukerche, H. A. B. F. Oliveira, E. F. Nakamura and A. A. F. Loureiro, "Localization systems for wireless sensor networks," *IEEE Wireless Commun.*, vol. 14, no. 6, pp. 6-12, Dec. 2007.
[3] S. Liu, L. Liu, J. Tang, B. Yu, Y. Wang and W. Shi, "Edge Computing for Autonomous Driving: Opportunities and Challenges," *Proceedings of the IEEE*, vol. 107, no. 8, pp. 1697-1716, Aug. 2019.
[4] Y. Cao, Y. Zhao and F. Dai, "Node Localization in Wireless Sensor Networks Based on Quantum Annealing Algorithm and Edge Computing," *2019 International Conference on Internet of Things (iThings) and IEEE Green Computing and Communications (GreenCom) and IEEE Cyber, Physical and Social Computing (CPSCom) and IEEE Smart Data (SmartData)*, Atlanta, GA, USA, 2019, pp. 564-568.
[5] L. Jiang, M. Cheng and T. Matsumoto, "A TOA-DoA Hybrid Factor Graph-based Technique for Multi-target Geolocation and Tracking," *IEEE Access*, vol. 9, pp. 14203-14215, 2021.
[6] J. Meyer-Hilberg and T. Jacob, "High accuracy navigation and landing system using GPS/IMU system integration," *IEEE Aerospace and Electronic Systems Magazine*, vol. 9, no. 7, pp. 11-17, July 1994.
[7] M. Atif, R. Ahmad, W. Ahmad, L. Zhao and J. J. P. C. Rodrigues, "UAV-Assisted Wireless Localization for Search and Rescue," *IEEE Systems Journal*, vol. 15, no. 3, pp. 3261-3272, Sept. 2021.
[8] G. Bresson, Z. Alsayed, L. Yu and S. Glaser, "Simultaneous Localization and Mapping: A Survey of Current Trends in Autonomous Driving," *IEEE Trans. Intelligent Vehicles*, vol. 2, no. 3, pp. 194-220, Sept. 2017.
[9] N. M. Drawil, H. M. Amar and O. A. Basir, "GPS Localization Accuracy Classification: A Context-Based Approach," *IEEE Trans. Intelligent Transportation Syst.*, vol. 14, no. 1, pp. 262-273, March 2013.
[10] Yiu-Tong Chan, Wing-Yue Tsui, Hing-Cheung So and Pak-chung Ching, "Time-of-arrival based localization under NLOS conditions," *IEEE Trans. Veh. Technol.*, vol. 55, no. 1, pp. 17-24, Jan. 2006.
[11] Jung-Chieh Chen, Yeong-Cheng Wang, Ching-Shyang Maa and Jiunn-Tsair Chen, "Network-side mobile position location using factor graphs," *IEEE Trans. Wireless Commun.*, vol. 5, no. 10, pp. 2696-2704, Oct. 2006.
[12] O. Ennasr, G. Xing and X. Tan, "Distributed time-difference-of-arrival (TDoA)-based localization of a moving target," *2016 IEEE 55th Conference on Decision and Control (CDC)*, Las Vegas, NV, USA, 2016, pp. 2652-2658.
[13] O. Ennasr and X. Tan, "Time-Difference-of-Arrival (TDoA)-Based Distributed Target Localization by A Robotic Network," *IEEE Trans. Control of Network Syst.*, vol. 7, no. 3, pp. 1416-1427, Sept. 2020.
[14] G. Wang, Y. Li and N. Ansari, "A Semidefinite Relaxation Method for Source Localization Using TDoA and FDoA Measurements," *IEEE Trans. Veh. Technol.*, vol. 62, no. 2, pp. 853-862, Feb. 2013.
[15] K. C. Ho and Y. T. Chan, "Solution and performance analysis of geolocation by TDoA," *IEEE Trans. Aerospace, Electron. Syst.*, vol. 29, no. 4, pp. 1311-1322, Oct. 1993.
[16] M. Cheng, M. R. K. Aziz and T. Matsumoto, "Integrated Factor Graph Algorithm for DoA-Based Geolocation and Tracking," *IEEE Access*, vol. 8, pp. 49989-49998, 2020.
[17] X. Zhou, L. Chen, J. Yan and R. Chen, "Accurate DoA Estimation With Adjacent Angle Power Difference for Indoor Localization," *IEEE Access*, vol. 8, pp. 44702-44713, 2020.
[18] D. N. Jayasimha, S. S. Iyengar and R. L. Kashyap, "Information integration and synchronization in distributed sensor networks," *IEEE Trans. Syst. Man, and Cybernetics*, vol. 21, no. 5, pp. 1032-1043, Sept.-Oct. 1991.
[19] R. Schmidt, "Multiple emitter location and signal parameter estimation," *IEEE Trans. Anten. and Propa.*, vol. 34, no. 3, pp. 276-280, Mar. 1986.
[20] R. Roy and T. Kailath, "ESPRIT-estimation of signal parameters via rotational invariance techniques," *IEEE Trans. Acoustics, Speech, Signal Process.*, vol. 37, no. 7, pp. 984-995, July 1989.
[21] B. D. Rao and K. V. S. Hari, "Performance analysis of Root-Music," *IEEE Trans. Acoust., Speech, and Signal Process.*, vol. 37, no. 12, pp. 1939-1949, Dec. 1989
[22] M. Haardt and J. A. Nossek, "Unitary ESPRIT: how to obtain increased estimation accuracy with a reduced computational burden," *IEEE Trans. Signal Process.*, vol. 43, no. 5, pp. 1232-1242, May. 1995.
[23] L. Jiang, N. Keerativoranan, T. Matsumoto, J. Takada, "Two-Dimensional Smoothing in the Presence of Empirical Non-stationarity for DoA Detection of Fast-Moving Target
Part I: Block-wise subspace-based technique", *IEEE Trans. Aerospace, Electron. Syst.* (under review)
[24] L. Jiang, N. Keerativoranan, T. Matsumoto, J. Takada, "Two-Dimensional Smoothing in the Presence of Empirical Non-stationarity for DoA Detection of Fast-Moving Target
Part II: Recursive subspace tracking by using LORAF", *IEEE Trans. Aerospace, Electron. Syst.* (under review)
[25] C. M. Mylonakis and Z. D. Zaharis, "A Novel Three-Dimensional Direction-of-Arrival Estimation Approach Using a Deep Convolutional Neural Network," *IEEE Open Journal of Vehicular Technology*, vol. 5, pp. 643-657, 2024.
[26] H. A. Kassir et al., "Improving DoA Estimation via an Optimal Deep Residual Neural Network Classifier on Uniform Linear Arrays," *IEEE Open Journal of Antennas and Propagation*, vol. 5, no. 2, pp. 460-473, April 2024.
[27] L. M. Kaplan, Qiang Le and N. Molnar, "Maximum likelihood methods for bearings-only target localization," *2001 IEEE International Conference on Acoustics, Speech, and Signal Processing. Proceedings (Cat. No.01CH37221)*, Salt Lake City, UT, USA, 2001, pp. 3001-3004 vol.5.
[28] W. H. Foy, "Position location solutions by Taylor-Series estimation," IEEE Trans. Aerosp. Electron. Syst., vol. 12, no. 2, pp. 187-193, Mar. 1976.
[29] M. R. K. Aziz, K. Anwar, and T. Matsumoto, "A new DoA-based factor graph geolocation technique for detection of unknown radio wave emitter position using the first-order Taylor series approximation," *EURASIP J. Wireless Commun. Netw.*, vol. 2016, no. 1, p.189, Aug. 2016.
[30] A. Azevedo, C. Bentes, M. C. Castro and C. Tadonki, "Performance Analysis and Optimization of the Vector-Kronecker Product Multiplication," *2020 IEEE 32nd International Symposium on Computer Architecture and High Performance Computing (SBAC-PAD)*, Porto, Portugal, 2020, pp. 265-272.
[31] P. Strobach, "Low-rank adaptive filters," *IEEE Trans. Signal Process.*, vol. 44, no. 12, pp. 2932-2947, Dec. 1996.
[32] L. Ljung, "Asymptotic behavior of the extended Kalman filter as a parameter estimator for linear systems," *IEEE Trans. Automatic Control*, vol. 24, no. 1, pp. 36-50, Feb. 1979.
[33] K. P. Sinaga and M. -S. Yang, "Unsupervised K-Means Clustering Algorithm," in IEEE Access, vol. 8, pp. 80716-80727, 2020.

LEI JIANG received the B.S. degree in electronic and information engineering from the University of Science and Technology LiaoNing, Liaoning, China, in 2017, the M.S. degree from Japan Advanced Institute of Science and Technology (JAIST), Ishikawa, Japan, in 2021. He is currently pursuing the Ph.D. degree in department of Transdisciplinary Science and Engineering, Tokyo Institute of Technology. His research interests include network information theory, iterative coding/decoding, wireless geolocation techniques, signal processing.

NOPPHON KEERATIVORANAN (Member, IEEE) was born in 1989. He received his B.E. degree (Hons.) in electrical engineering from Thammasat University, Thailand, in 2012, the M.S. degree from Seoul National University, South Korea, in 2015, and the D.E. degree from the Tokyo Institute of Technology, Japan. In 2012, he was a Telecommunication Engineer with Advance Info Service (AIS), Thailand. From 2015 to 2016, he was a Research Assistant with the National Electronics and Computer Technology Center (NECTEC), Thailand. He is currently a Researcher with the Tokyo Institute of Technology. His research interests include RF-based localization and tracking, radio propagation channel modeling, and measurements for wireless communication system and application.

TAD MATSUMOTO (Fellow, IEEE) received the B.S. and M.S. degrees in electrical engineering under the mentorship of Prof. S.-I. Takahashi, and the Ph.D. degree in electrical engineering under the supervision of Prof. M. Nakagawa from Keio University, Yokohama, Japan, in 1978, 1980, and 1991, respectively.,In 1980, he joined Nippon Telegraph and Telephone Corporation (NTT), where he was involved in a lot of research and development projects, all for mobile wireless communications systems. In 1992, he transferred to NTT DoCoMo, where he researched on code-division multiple-access techniques for mobile communication systems. In 1994, he transferred to NTT America, where he served as a Senior Technical Advisor of a joint project between NTT and NEXTEL Communications. From 1996 to 2001, he returned to NTT DoCoMo, where he served as the Head of the Radio Signal Processing Laboratory. He researched on adaptive signal processing, multiple-input multiple-output turbo signal detection, interference cancellation, and space-time coding techniques for broadband mobile communications. In 2002, he moved to the University of Oulu, Finland, where he served as a Professor with the Centre for Wireless Communications. In 2006, he served as a Visiting Professor with the Ilmenau University of Technology, Ilmenau, Germany, funded by the German MERCATOR Visiting Professorship Program. Since 2007, he has been serving as a Professor with the Japan Advanced Institute of Science and Technology, Japan, while also keeping a cross-appointment position with the University of Oulu.,Prof. Matsumoto is a member of IEICE. He was a recipient of the IEEE VTS Outstanding Service Award, in 2001, the Nokia Foundation Visiting Fellow Scholarship Award, in 2002, the IEEE Japan Council Award for Distinguished Service to the Society, in 2006, the IEEE Vehicular Technology Society James R. Evans Avant Garde Award, in 2006, the Thuringen State Research Award for Advanced Applied Science, in 2006, the 2007 Best paper Award of Institute of Electrical, Communication, and Information Engineers of Japan, in 2008, the Telecom System Technology Award by the Telecommunications Advancement Foundation, in 2009, the IEEE Communication Letters Exemplary Reviewer, in 2011, the Nikkei Wireless Japan Award, in 2013, the IEEE VTS Recognition for Outstanding Distinguished Lecturer, in 2016, and the IEEE Transactions on Communications Exemplary Reviewer, in 2018. He has led a lot of projects funded by Academy-of-Finland, European FP7, and the Japan Society for the Promotion of Science and by Japanese private companies. He has been appointed as a Finland Distinguished Professor from 2008 to 2012, funded by the Finnish National Technology Agency (Tekes) and Finnish Academy, under which he preserves the rights to participate in and apply to European and Finnish national projects. He has been serving as an IEEE Vehicular Technology Distinguished Speaker, since 2016.

JUN-ICHI TAKADA (Member, IEEE) received the B.E., M.E., and D.E. degrees in electrical and electronic engineering from the Tokyo Institute of Technology, Tokyo, Japan, in 1987, 1989, and 1992, respectively. He was a Research Associate with Chiba University, Chiba, Japan, from 1992 to 1994. He was an Associate Professor with the Tokyo Institute of Technology, from 1994 to 2006. He was also a Researcher with the National Institute of Information and Communications Technology, Kanagawa, Japan, from 2003 to 2007. He has been a Professor with the Tokyo Institute of Technology, since 2006. His research interests include radio-wave propagation and channel modeling for mobile and short-range wireless systems, regulatory issues of spectrum sharing, and ICT applications for international development. He is a Fellow of the IEICE, Japan.